ADVANCED MATERIALS
www.advmat.de

Linker Engineering of Sandwich-Structured Metal–Organic Framework Composites for Optimized Photocatalytic H_2 Production

Siyuan Wang, Zhiwen Ai, Xinwei Niu, Weijie Yang, Rong Kang, Zhongyuan Lin, Amir Waseem, Long Jiao, and Hai-Long Jiang**

While the microenvironment around catalytic sites is recognized to be crucial in thermocatalysis, its roles in photocatalysis remain subtle. In this work, a series of sandwich-structured metal–organic framework (MOF) composites, UiO-66-NH_2@Pt@UiO-66-X (X means functional groups), is rationally constructed for visible-light photocatalytic H_2 production. By varying the —X groups of the UiO-66-X shell, the microenvironment of the Pt sites and photosensitive UiO-66-NH_2 core can be simultaneously modulated. Significantly, the MOF composites with identical light absorption and Pt loading present distinctly different photocatalytic H_2 production rates, following the —X group sequence of —H > —Br > —NA (naphthalene) > —OCH_3 > —Cl > —NO_2. UiO-66-NH_2@Pt@UiO-66-H demonstrates H_2 production rate up to 2708.2 μmol g^{-1} h^{-1}, ≈222 times that of UiO-66-NH_2@Pt@UiO-66-NO_2. Mechanism investigations suggest that the variation of the —X group can balance the charge separation of the UiO-66-NH_2 core and the proton reduction ability of Pt, leading to an optimal activity of UiO-66-NH_2@Pt@UiO-66-H at the equilibrium point.

1. Introduction

Solar-powered photocatalytic hydrogen production is considered to be a viable solution to the global energy crisis and the exploration of efficient artificial photocatalysts is regarded as one of the most critical issues in this field.[1,2] Among various catalyst systems, natural enzymes present ultrahigh catalytic efficiency for many challenging reactions under mild conditions, attributed to the synergistic effect between catalytic sites and their surrounding microenvironments.[3] Learned from enzyme catalysis, the fabrication of suitable microenvironments around catalytic sites should also be of great significance in heterogeneous catalysis for enhanced performance which has been proved in thermocatalysis.[4] Nevertheless, compared with thermocatalysis, photocatalysis, as another kind of heterogeneous catalysis, usually suffers from more complicated processes (photoexcitation, charge separation, and surface reaction) that are mutually entangled,[5] giving rise to the challenge toward photocatalytic performance optimization by microenvironment modulation. To meet this challenge, it is of great significance to construct a suitable material platform, where the local microenvironment around both photosensitizer and catalytic units can be regulated at atomic precision for enhanced photocatalysis.

Metal–organic frameworks (MOFs),[6,7] a class of promising porous crystalline materials constructed by metal nodes and organic ligands, have attracted extensive interests in heterogeneous catalysis.[8] Especially, due to the atomically precise structures, modifiable pore environment, and semiconductor-like behavior, MOFs have demonstrated their great potential in photocatalysis.[9] Moreover, the well-defined and easily tailorable components and structures of MOFs greatly facilitate the precise microenvironment modulation at an atomic scale.[4d,10] Meanwhile, the high porosity in MOFs enables the good accessibility of catalytic metal centers, regardless of their location on the skeleton or in the pore space.[11] Additionally, some MOF composites with novel structures, such as sandwich-like, core-shell and yolk-shell structures, have been successfully synthesized and complex functionalities have been reported toward catalysis.[12] On account of these, MOFs would be a promising model to investigate the significant roles of microenvironment modulation in photocatalysis. Among

S. Wang, Z. Ai, R. Kang, Z. Lin, L. Jiao, H.-L. Jiang
Hefei National Research Center for Physical Sciences at the Microscale
Department of Chemistry
Collaborative Innovation Center of Chemistry for Energy Materials (iChEM)
University of Science and Technology of China
Hefei, Anhui 230026, P. R. China
E-mail: longjiao@ustc.edu.cn; jianglab@ustc.edu.cn
X. Niu, W. Yang
School of Energy and Power Engineering
North China Electric Power University
Baoding, Hebei 071003, P. R. China
A. Waseem
Department of Chemistry
Quaid-i-Azam University
Islamabad 45320, Pakistan

The ORCID identification number(s) for the author(s) of this article can be found under https://doi.org/10.1002/adma.202302512

DOI: 10.1002/adma.202302512

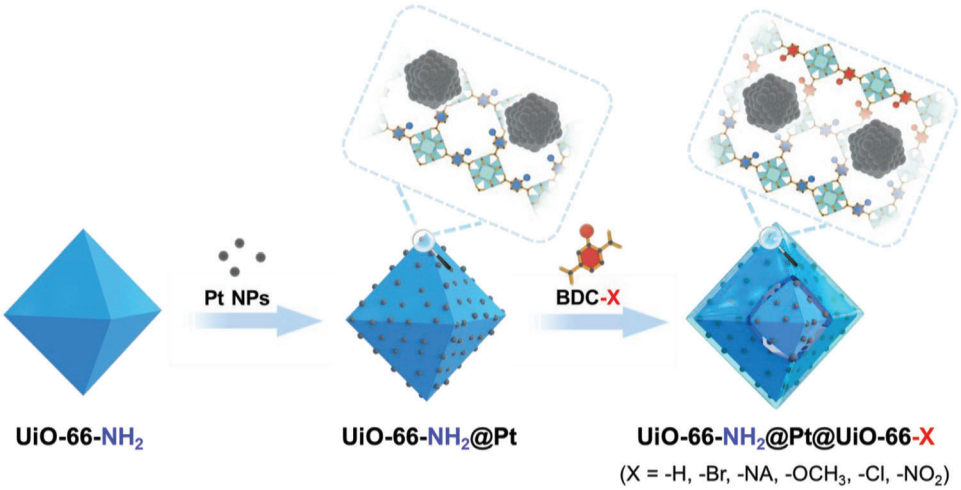

Scheme 1. Schematic illustration of the stepwise synthesis of sandwich-structured UiO-66-NH_2@Pt@UiO-66-X (X = —H, —Br, —NA, —OCH_3, —Cl, —NO_2) composites.

diverse MOFs, UiO-66-type MOFs, with excellent structural tailorability and stability, have been widely used in photocatalysis and should be a promising platform for microenvironment modulation.[13]

In this work, the pre-synthesized Pt NPs are attached on the outer surface of an as-prepared MOF, UiO-66-NH_2, to give UiO-66-NH_2@Pt via electrostatic self-assembly (**Scheme 1**). Following epitaxial growth, a series of isoreticular UiO-66-X shells with diverse functional groups are successfully coated on UiO-66-NH_2@Pt, affording UiO-66-NH_2@Pt@UiO-66-X (X = —H, —Br, —NA (naphthalene for short), —OCH_3, —Cl, —NO_2) composites with sandwich-like structure (Scheme 1). Such a structure guarantees the sufficient contact of UiO-66-X shell with both UiO-66-NH_2 core and Pt NPs, facilitating the precise regulation of UiO-66-NH_2 and Pt NPs by simply altering the —X group of the shell MOF as the microenvironment. As a result, UiO-66-NH_2@Pt@UiO-66-H presents the best activity among all UiO-66-NH_2@Pt@UiO-66-X and UiO-66-NH_2@Pt in photocatalytic H_2 production with trimethylamine (TEA) as the electron donor, highlighting the critical role of UiO-66-X shells in performance regulation. Mechanism investigations reveal that UiO-66-X shell, serving as the microenvironment parameter, reversely regulates the exciton binding energy of UiO-66-NH_2 (photosensitizer) core and proton reduction rate on Pt (cocatalyst), and thereby UiO-66-NH_2@Pt@UiO-66-H locating at the equilibrium point possesses the optimal photocatalytic activity.

2. Results and Discussion

2.1. Synthesis and Structural Characterizations

The typical Zr-based MOF, UiO-66-NH_2 presents the octahedral morphology with size ≈370 nm were synthesized (**Figure 1**a; Figure S1, Supporting Information). Meanwhile, Pt NPs with an average size of 3.8 nm were prepared under the stabilization of poly(vinylpyrrolidone) (PVP) and subsequently assembled onto the outer surface of the as-prepared UiO-66-NH_2 via electrostatic interaction, affording UiO-66-NH_2@Pt composite with inherited MOF crystallinity and morphology (Figures S1–S3, Supporting Information). After that, a series of isoreticular UiO-66-X layers with different functional groups were epitaxially grown on UiO-66-NH_2@Pt to afford UiO-66-NH_2@Pt@UiO-66-X (X = —H, —Br, —NA, —OCH_3, —Cl, —NO_2) composites, in which Pt NPs were sandwiched. Due to the similar lattice parameters of UiO-66-X shells to the UiO-66-NH_2 core, the resultant UiO-66-NH_2@Pt@UiO-66-X composites show well-retained crystallinity and octahedral morphology (Figure 1b; Figures S4 and S5, Supporting Information). Transmission electron microscopy (TEM) observation demonstrates that Pt NPs in UiO-66-NH_2@Pt@UiO-66-X are located between the MOF core and UiO-66-X shells (Figure 1c,d; Figures S6–S10, Supporting Information), and such a sandwich-like structure maximizes the contact of UiO-66-X shell with both UiO-66-NH_2 and Pt. Moreover, the thickness of UiO-66-X shell is well controlled at ≈20 nm for all UiO-66-NH_2@Pt@UiO-66-X composites (Figure 1d; Figures S6–S10, Supporting Information).

Nitrogen adsorption suggests the highly porous feature of all composites (Figure S11, Supporting Information), favorable to the accessibility of Pt NPs. Moreover, UV–vis diffuse reflectance spectra of all UiO-66-NH_2@Pt@UiO-66-X composites show almost the same profiles for light responses with very similar bandgaps, in consistent with the pristine UiO-66-NH_2 (**Figure 2**a,b; Figures S12 and S13 and Table S1, Supporting Information). Moreover, the Pt loading in UiO-66-NH_2@Pt@UiO-66-X composites is very similar to ≈1.9 wt% according to inductively coupled plasma atomic emission spectroscopy (ICP-AES) analysis (Figure 2b; Table S2, Supporting Information). Based on the results above, it can be seen that, except for the different —X functional groups on the shell MOF, all UiO-66-NH_2@Pt@UiO-66-X composites present comparable sandwich-like structure, shell thickness, Pt loading, and light absorption, providing ideal models to investigate the influence of the microenvironment created by the shell MOFs with diverse —X groups on the resulting photocatalytic activity. Furthermore, other kinds of

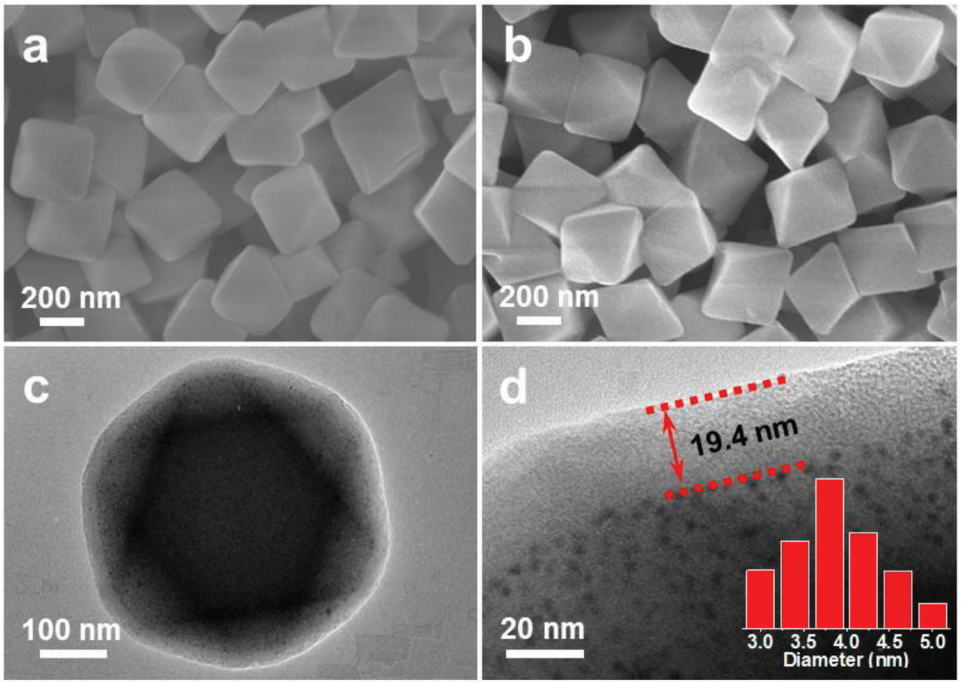

Figure 1. a,b) Scanning electron microscopy (SEM) images of UiO-66-NH_2 (a) and UiO-66-NH_2@Pt@UiO-66-H (b). c) TEM and d) enlarged TEM images of UiO-66-NH_2@Pt@UiO-66-H (inset of (d): size distribution of Pt NPs).

sandwich-like MOF composite, such as ZIF-8@Pt@ZIF-67 and MIL-125-NH_2@Pt@MIL-125-NH_2, have also been constructed successfully, illustrating the universality of epitaxial growth technique on the fabrication of sandwich-like MOF composite (Figure S14, Supporting Information).

2.2. Photocatalytic Performance Evaluation for H_2 Production

Inspired by the results above, photocatalytic H_2 production over UiO-66-NH_2@Pt@UiO-66-X was investigated under visible light irradiation and TEA acts as electron donor. As expected, the UiO-66-NH_2@Pt@UiO-66-X catalysts, with only variation in the —X groups on the shell MOFs, exhibit distinctly different photocatalytic hydrogen production rates following the replaceable group sequence of —H > —Br > —NA > —OCH_3 > —Cl > —NO_2 (Figure 2c). Specifically, UiO-66-NH_2@Pt@UiO-66-H possesses the highest hydrogen production rate up to 2708.2 μmol g^{-1} h^{-1}, which is ≈222 times and 4.9 times higher than that of UiO-66-NH_2@Pt@UiO-66-NO_2 (12.2 μmol g^{-1} h^{-1}) and UiO-66-NH_2@Pt without shell MOF (556.4 μmol g^{-1} h^{-1}), respectively, clearly highlighting the critical role of microenvironment created by the UiO-66-X (Figure 2c). The good crystallinity of all the composite photocatalysts can be maintained after reaction (Figure S15, Supporting Information). Moreover, the best-performing UiO-66-NH_2@Pt@UiO-66-H shows a stable photocatalytic H_2 production rate during six consecutive runs (Figure 2d). As controls, the photocatalytic H_2 production of UiO-66-NH_2 and UiO-66-NH_2@UiO-66-X without Pt has been examined, both of which present negligible H_2 production rates, confirming the significant role of Pt serving as catalytic site (Table S3, Supporting Information). In addition, UiO-66 without the —NH_2 group, which gives no response to visible light, is also employed as core instead of UiO-66-NH_2 to afford UiO-66@Pt@UiO-66-X composites (Figures S3 and S16, Supporting Information). It can be seen that no H_2 is produced over UiO-66@Pt@UiO-66-X under visible-light irradiation (Table S4, Supporting Information), given their light response ability in the UV region only (Figure S16, Supporting Information), revealing the necessity of the UiO-66-NH_2 core as photosensitizer and excluding the possible light harvesting contributed by the UiO-66-X shell. Furthermore, UiO-66-NH_2@UiO-66-H@Pt with Pt on the outer surface of the shell is further constructed as a control, which presents much inferior performance to UiO-66-NH_2@Pt@UiO-66-H, indicating the significance of Pt location to accept photo-generated electrons from UiO-66-NH_2 core (Figures S17–S19, Supporting Information). In addition, triethanolamine (TEOA), another typical electron donor, has also been employed instead of TEA. It can be seen that the photocatalytic activities of UiO-66-NH_2@Pt@UiO-66-X series using both TEA and TEOA present the same trend along with the variation of —X group, excluding the potential influence of electron donors on the activity sequence (Figure S20, Supporting Information).

Moreover, the solvent effect of photocatalytic performance has also been studied and results show that the photocatalytic activity of UiO-66-NH_2@Pt@UiO-66-H in the mixture of acetonitrile/TEA/H_2O is much higher than those in the mixture of acetonitrile/TEA and TEA/H_2O (Figure S21, Supporting Information). The water can be directly involved in hydrogen production as a hydrogen source, and acetonitrile guarantees the good dispersion of MOF with hydrophic ligands as well as activates H_2O molecules via hydrogen-bonding interaction.[14] As a result, the acetonitrile and H_2O are proved to be necessary for optimizing catalytic performance.

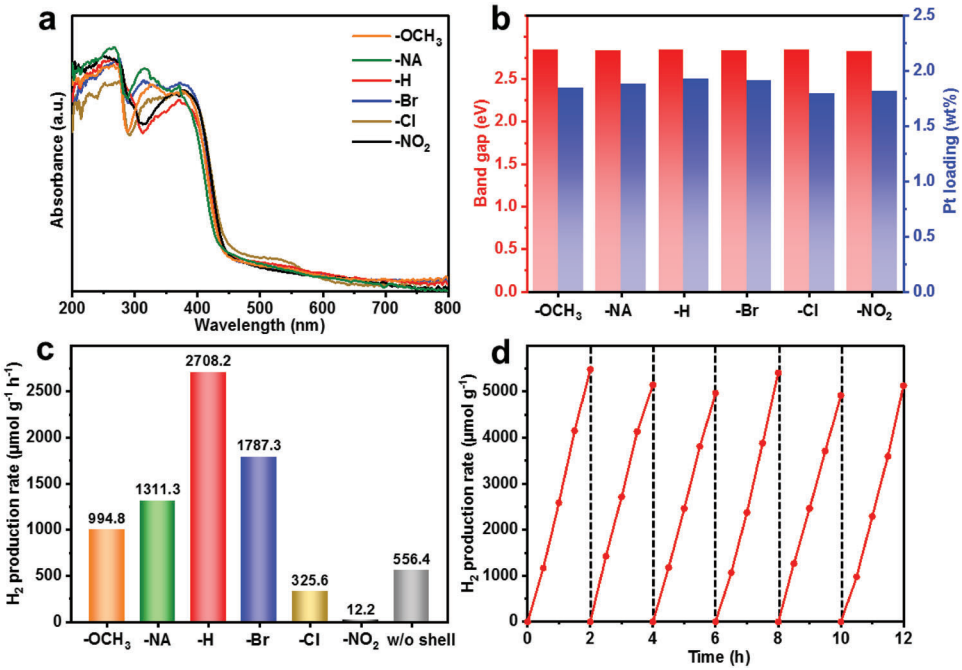

Figure 2. a) UV–vis spectra and b) bandgap and Pt loading values for UiO-66-NH_2@Pt@UiO-66-X composites. c) Photocatalytic hydrogen production rates of UiO-66-NH_2@Pt@UiO-66-X (labeled —X) and UiO-66-NH_2@Pt without shell (labeled w/o shell). d) Photocatalytic recyclability of UiO-66-NH_2@Pt@UiO-66-H.

2.3. Mechanism Investigations

In view of the remarkable activity differences among UiO-66-NH_2@Pt@UiO-66-X composites, related characterizations have been carried out to clarify the intrinsic mechanism. Considering the multiple processes in the photocatalytic reaction, the efficiencies of optical absorption (η_1), charge separation (η_2), and surface reaction (η_3) are regarded as dominant factors that synergistically affect the overall photocatalytic efficiency (η_{sum}) according to the equation, $\eta_{sum} = \eta_1 \times \eta_2 \times \eta_3$, and the higher η_{sum} manifests better activity.[15] On account of this, the specific roles of the UiO-66-X shell in the photocatalytic activity regulation of UiO-66-NH_2@Pt@UiO-66-X are investigated by the above three aspects. Given the photosensitizer for all the composites is from the same core, UiO-66-NH_2, the optical absorption (η_1) is unified, and the activity difference should be ascribed to charge separation (η_2) and surface reaction (η_3).

Exciton binding energy (E_b), a key parameter to evaluate charge separation efficiency (η_2) of photocatalysts, has been determined by temperature-dependent photoluminescence (PL) spectra.[16] With decreased temperature, the PL intensities of UiO-66-NH_2@Pt@UiO-66-X increase monotonically, which can be further fitted to quantify the values of E_b (**Figure 3**a; Figures S22–S26, Supporting Information). Accordingly, the calculated E_b values for UiO-66-NH_2@Pt@UiO-66-X (X = —H, —Br, —NA, —OCH_3, —Cl, —NO_2) follow the sequence —OCH_3 (75.2 meV) > —NA (71.9 meV) > —H (67.6 meV) > —Br (62.1 meV) > —Cl (48.4 meV) > —NO_2 (45.3 meV) (Figure 3b; Figures S22–S26 and Table S5, Supporting Information). Since the smaller E_b corresponds to the higher charge separation efficiency (η_2), it is suggested that η_2 follows a sequence of —OCH_3 < —NA < —H < —Br < —Cl < —NO_2, positively correlated with the electron-withdrawing degree of these groups, which indicates that UiO-66-NH_2@Pt@UiO-66-NO_2 possesses the highest charge separation ability (Figure 3b,c).[17] Moreover, the E_b values of core-shell UiO-66-NH_2@UiO-66-X in the absence of Pt also follow the same trend as UiO-66-NH_2@Pt@UiO-66-X (Figures S27–S33; and Table S6, Supporting Information), clearly demonstrating the regulation ability of UiO-66-X shell for the charge separation of the UiO-66-NH_2 core. Meanwhile, PL emission spectra and time-resolved PL spectra jointly manifest the weaker fluorescence intensity and shorter exciton lifetime for UiO-66-NH_2@Pt@UiO-66-X involving the —X functional group with increased electron-withdrawing ability (Figure 3d; Figure S34 and Table S7, Supporting Information), supporting the enhanced exciton dissociation and charge separation, in agreement with the above E_b results.[18] It is worth noting that the E_b value of UiO-66-NH_2@Pt@UiO-66-X alone cannot correlate with the trend of photocatalytic activity, inferring that the charge separation efficiency (η_2) might not be the only factor dominating the photocatalytic performance (Figure S35, Supporting Information).

Furthermore, the properties of Pt cocatalyst covered with UiO-X shells, which would be associated with the efficiency of surface reaction process (η_3), have been further characterized. X-ray photoelectron spectroscopy (XPS) analysis suggests that the Pt electron density in UiO-66-NH_2@Pt@UiO-66-X follows the sequence of —NO_2 < —Cl < —Br < —H < —NA < —OCH_3, in line with the increase of electron-donating ability of the —X functional group (**Figure 4**a). Moreover, CO adsorption diffuse reflectance infrared Fourier transform spectroscopy (DRIFTS) has been conducted to evaluate the electron density of Pt. It can be

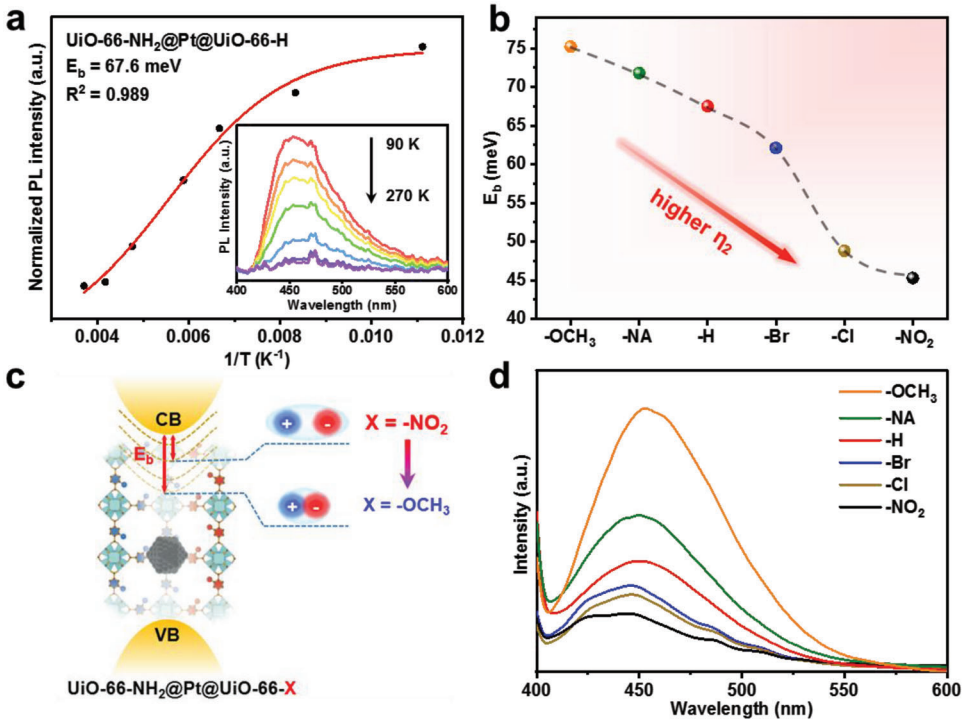

Figure 3. a) Integrated PL emission intensity of UiO-66-NH_2@Pt@UiO-66-H as a function of reciprocal temperature (inset: temperature-dependent PL spectra, λ_{ex} = 380 nm). b) The gradually decreased E_b values of UiO-66-NH_2@Pt@UiO-66-X along with the increased electron-withdrawing ability of —X group. c) Schematic illustration showing the exciton states with different E_b of UiO-66-NH_2@Pt@UiO-66-X. d) PL emission spectra (λ_{ex} = 380 nm) for UiO-66-NH_2@Pt@UiO-66-X.

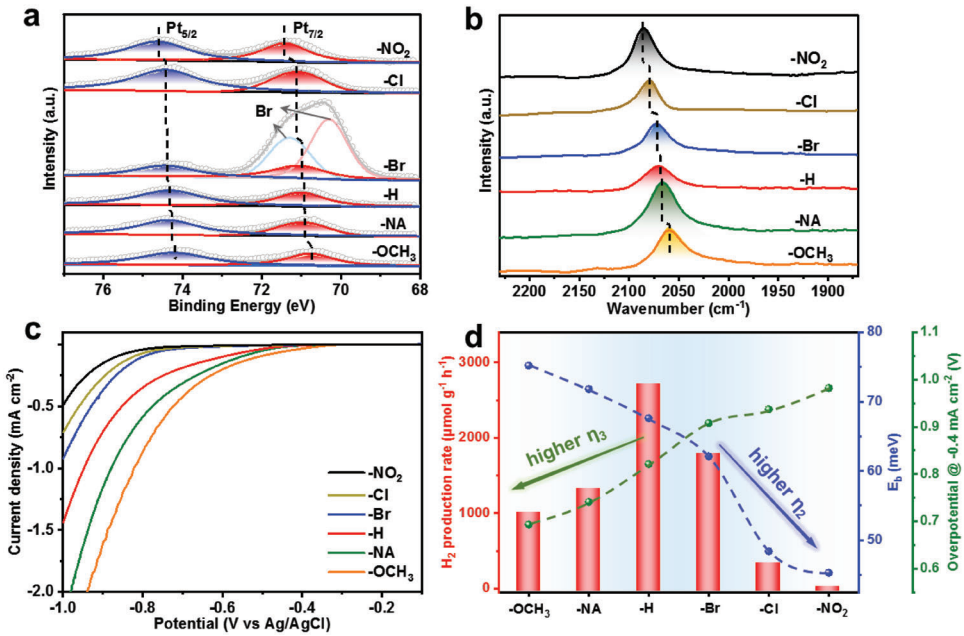

Figure 4. a) Pt 4f XPS spectra, b) CO adsorption DRIFT spectra, and c) electrochemical LSV curves for HER of UiO-66-NH_2@Pt@UiO-66-X composites. d) The variation of H_2 production rate, E_b and overpotential for HER of UiO-66-NH_2@Pt@UiO-66-X involving the —X functional group with gradually increasing electron-withdrawing ability.

seen that redshift of the CO adsorption peak occurs to the UiO-66-NH_2@Pt@UiO-66-X composites, gradually from 2085 cm^{-1} (—NO_2) to 2059 cm^{-1} (—OCH_3), supporting the increased Pt electron density along with improved electron-donating ability of —X functional group (—NO_2 < —Cl < —Br < —H < —NA < —OCH_3) (Figure 4b),[19] in accordance with the above XPS results. The intrinsic proton reduction ability of Pt surface in the composites was evaluated by electrochemical hydrogen evolution reaction (HER) measurements. The value of overpotential decreased along with increased Pt electron density, which supports the above XPS and DRIFTS results, indicating that surface reaction efficiency (η_3) presents an order of —OCH_3 > —NA > —H > —Br > —Cl > —NO_2 (Figure 4c; Figure S36, Supporting Information), in reverse correlation with electron-withdrawing ability of the —X functional group. In addition, the density functional theory (DFT) calculations further reveal that the Pt sites covered by —X groups with higher electron-donating ability possess lower values of $|\Delta G_{H^*}|$ corresponding to higher η_3, which is consistent with the results of electrochemical HER measurements (Figure 4c; Figures S37 and S38, Supporting Information).

In combination with the results above, with gradually increasing electron-withdrawing ability of the —X group (—OCH_3 < —NA < —H < —Br < —Cl < —NO_2), the charge separation efficiency (η_2) is improved, while the intrinsic proton reduction efficiency (η_3) of Pt is suppressed, as evaluated by the E_b and overpotential for HER (Figure 4d). Given the trade-off effect between the charge separation efficiency (η_2) and proton reduction efficiency of Pt (η_3), the —X group with too strong electron-withdrawing or -donating ability on the shell MOF is unfavorable for the resulting photocatalytic activity. Similar to the Sabatier principle, it is reasonable that the photocatalytic H_2 production rate presents a volcano-like profile along with the electron-withdrawing/donating ability of the —X group (Figure 4d). To our delight, by the mathematical simulation, the volcano-like plot of η_{sum} can be visually presented (Figure S39, Supporting Information), which is highly consistent with the volcano-like activity trend in experiments (Figure 4d). The UiO-66-NH_2@Pt@UiO-66-H, featuring the moderate electron-donating/withdrawing ability of the —H group, balances the charge separation efficiency and the proton reduction ability of Pt, resulting in the highest photocatalytic activity (Figure 4d).

3. Conclusion

A versatile epitaxial growth strategy has been developed for the fabrication of sandwich-structured MOF@Pt@MOF composites, namely UiO-66-NH_2@Pt@UiO-66-X (X = —H, —Br, —NA, —OCH_3, —Cl, —NO_2), featuring similar structure, shell thickness, light harvesting ability and Pt loading, toward photocatalytic H_2 production. The isoreticular UiO-X shell enables the modulation of microenvironment properties of both Pt cocatalyst and UiO-66-NH_2 photosensitizer in UiO-66-NH_2@Pt@UiO-66-X, by simply altering the —X group without disturbing other structural parameters. As a result, UiO-66-NH_2@Pt@UiO-66-H presents the highest H_2 production rate up to 2708.2 μmol g^{-1} h^{-1}, ≈222 and 2.7 times higher than UiO-66-NH_2@Pt@UiO-66-NO_2 (with the most electron-withdrawing group) and UiO-66-NH_2@Pt@UiO-66-OCH_3 (with the most electron-donating group). Mechanism analysis reveals that too strong electron-donating ability of the —X group in the shell MOF will impede charge separation of UiO-66-NH_2 core, while too stong electron-withdrawing ability inhibits the proton reduction on Pt, leading to a non-linear relevance between the resulting H_2 production activity and the electron-withdrawing/-donating ability of the —X group. The results unambiguously highlight the strong power of microenvironment modulation by the shell MOF. Therefore, UiO-66-NH_2@Pt@UiO-66-H, with a moderate electron-push/-pull effect on the linker, can balance the charge separation and the Pt proton reduction ability, affording the optimal catalytic performance. This work provides a new principle in the design of efficient photocatalysts and sheds light on the dual regulation of charge separation and reaction efficiency in photocatalysis by tailoring the microenvironment.

Supporting Information

Supporting Information is available from the Wiley Online Library or from the author.

Acknowledgements

This work was supported by the National Key Research and Development Program of China (2021YFA1500402), the Strategic Priority Research Program of the Chinese Academy of Sciences (XDB0450302), the National Natural Science Foundation of China (22161142001, 22222507, 22001242), the International Partnership Program of CAS (123GJHZ2022028MI), and the Fundamental Research Funds for the Central Universities (WK3450000007, WK2060000038, WK2060000040). A.W. would like to thank the Pakistan Science Foundation for funding the Pak/China project No. PSF/NSFC-IV/CHEM/C-QAU (27).

Conflict of Interest

The authors declare no conflict of interest.

Data Availability Statement

The data that support the findings of this study are available from the corresponding author upon reasonable request.

Keywords

hydrogen production, linker engineering, metal–organic frameworks, photocatalysis

Received: March 18, 2023
Revised: May 18, 2023
Published online: August 4, 2023

[1] a) H. Nishiyama, T. Yamada, M. Nakabayashi, Y. Maehara, M. Yamaguchi, Y. Kuromiya, Y. Nagatsuma, H. Tokudome, S. Akiyama, T. Watanabe, R. Narushima, S. Okunaka, N. Shibata, T. Takata, T. Hisatomi, K. Domen, *Nature* **2021**, *598*, 304; b) F. Guo, J.-H. Guo, P. Wang, Y.-S. Kang, Y. Liu, J. Zhao, W.-Y. Sun, *Chem. Sci.* **2019**, *10*, 4834; c) S. Guo, L.-H. Kong, P. Wang, S. Yao, T.-B. Lu, Z.-M. Zhang, *Angew. Chem., Int. Ed.* **2022**, *61*, 202206193.

[2] a) X.-B. Li, Z.-K. Xin, S.-G. Xia, X.-Y. Gao, C.-H. Tung, L.-Z. Wu, *Chem. Soc. Rev.* **2020**, *49*, 9028; b) G. Zhao, Y. Sun, W. Zhou, X. Wang, K. Chang, G. Liu, H. Liu, T. Kako, J. Ye, *Adv. Mater.* **2017**, *29*, 1703258.

[3] a) R. Balasubramanian, S. M. Smith, S. Rawat, L. A. Yatsunyk, T. L. Stemmler, A. C. Rosenzweig, *Nature* **2010**, *465*, 115; b) M. Vázquez-González, C. Wang, I. Willner, *Nat. Catal.* **2020**, *3*, 256.

[4] a) A. R. Riscoe, C. J. Wrasman, A. A. Herzing, A. S. Hoffman, A. Menon, A. Boubnov, M. Vargas, S. R. Bare, M. Cargnello, *Nat. Catal.* **2019**, *2*, 852; b) A. Grigoropoulos, A. I. McKay, A. P. Katsoulidis, R. P. Davies, A. Haynes, L. Brammer, J. Xiao, A. S. Weller, M. J. Rosseinsky, *Angew. Chem., Int. Ed.* **2018**, *57*, 4532; c) X. Li, T. W. Goh, L. Li, C. Xiao, Z. Guo, X.-C. Zeng, W. Huang, *ACS Catal.* **2016**, *6*, 3461; d) L. Jiao, J. Wang, H.-L. Jiang, *Acc. Mater. Res.* **2021**, *2*, 327.

[5] a) H. Wang, L. Zhang, Z. Chen, J. Hu, S. Li, Z. Wang, J. Liu, X. Wang, *Chem. Soc. Rev.* **2014**, *43*, 5234; b) B. Pattengale, S. Yang, J. Ludwig, Z. Huang, X. Zhang, J. Huang, *J. Am. Chem. Soc.* **2016**, *138*, 8072; c) N.-Y. Huang, H. He, S. Liu, H.-L. Zhu, Y.-J. Li, J. Xu, J.-R. Huang, X. Wang, P.-Q. Liao, X.-M. Chen, *J. Am. Chem. Soc.* **2021**, *143*, 17424.

[6] a) H. Furukawa, K. E. Cordova, M. O'Keeffe, O. M. Yaghi, *Science* **2013**, *341*, 1230444; b) H.-C. Zhou, S. Kitagawa, *Chem. Soc. Rev.* **2014**, *43*, 5415; c) J. Liu, T. A. Goetjen, Q. Wang, J. G. Knapp, M. C. Wasson, Y. Yang, Z. H. Syed, M. Delferro, J. M. Notestein, O. K. Farha, J. T. Hupp, *Chem. Soc. Rev.* **2022**, *51*, 1045.

[7] a) X. Zhao, Y. Wang, D.-S. Li, X. Bu, P. Feng, *Adv. Mater.* **2018**, *30*, 1705189; b) B. Li, H.-M. Wen, Y. Cui, W. Zhou, G. Qian, B. Chen, *Adv. Mater.* **2016**, *28*, 8819; c) A. Kirchon, L. Feng, H. F. Drake, E. A. Joseph, H.-C. Zhou, *Chem. Soc. Rev.* **2018**, *47*, 8611.

[8] a) J. Zhu, P.-Z. Li, W. Guo, Y. Zhao, R. Zou, *Coord. Chem. Rev.* **2018**, *359*, 80; b) L. Jiao, Y. Wang, H.-L. Jiang, Q. Xu, *Adv. Mater.* **2018**, *30*, 1703663; c) P. M. Stanley, J. Haimerl, N. B. Shustova, R. A. Fischer, J. Warnan, *Nat. Chem.* **2022**, *14*, 1342; d) Y.-B. Huang, J. Liang, X.-S. Wang, R. Cao, *Chem. Soc. Rev.* **2017**, *46*, 126; e) A. Bavykina, N. Kolobov, I. S. Khan, J. A. Bau, A. Ramirez, J. Gascon, *Chem. Rev.* **2020**, *120*, 8468; f) S. Navalon, A. Dhakshinamoorthy, M. Alvaro, B. Ferrer, H. Garcia, *Chem. Rev.* **2023**, *123*, 445; g) J. Du, F. Li, L.-C. Sun, *Chem. Soc. Rev.* **2021**, *50*, 2663; h) J. Guo, Y. Qin, Y. Zhu, X. Zhang, C. Long, M. Zhao, Z. Tang, *Chem. Soc. Rev.* **2021**, *50*, 5366.

[9] a) J.-K. Jin, K. Wu, X.-Y. Liu, G.-Q. Huang, Y.-L. Huang, D. Luo, M. Xie, Y. Zhao, W. Lu, X.-P. Zhou, J. He, D. Li, *J. Am. Chem. Soc.* **2021**, *143*, 21340; b) Y. Fu, D. Sun, Y. Chen, R. Huang, Z. Ding, X. Fu, Z. Li, *Angew. Chem., Int. Ed.* **2012**, *51*, 3364; c) H. Hu, Z. Wang, L. Cao, L. Zeng, C. Zhang, W. Lin, C. Wang, *Nat. Chem.* **2021**, *13*, 358; d) F.-M. Zhang, J.-L. Sheng, Z.-D. Yang, X.-J. Sun, H.-L. Tang, M. Lu, H. Dong, F.-C. Shen, J. Liu, Y.-Q. Lan, *Angew. Chem., Int. Ed.* **2018**, *57*, 12106; e) Q. Mo, L. Zhang, S. Li, H. Song, Y. Fan, C.-Y. Su, *J. Am. Chem. Soc.* **2022**, *144*, 22747.

[10] a) Y. Zhang, Q. Zhou, Z.-F. Qiu, X.-Y. Zhang, J.-Q. Chen, Y. Zhao, F. Gong, W.-Y. Sun, *Adv. Funct. Mater.* **2022**, *32*, 2203677; b) D. Chen, W. Yang, L. Jiao, L. Li, S.-H. Yu, H.-L. Jiang, *Adv. Mater.* **2020**, *32*, 2000041; c) G. Lan, Y. Fan, W. Shi, E. You, S. S. Veroneau, W. Lin, *Nat. Catal.* **2022**, *5*, 1006.

[11] a) H. Zhang, J. Wei, J. Dong, G. Liu, L. Shi, P. An, G. Zhao, J. Kong, X. Wang, X. Meng, J. Zhang, J. Ye, *Angew. Chem., Int. Ed.* **2016**, *128*, 14522; b) L.-Y. Wu, Y.-F. Mu, X.-X. Guo, W. Zhang, Z.-M. Zhang, M. Zhang, T.-B. Lu, *Angew. Chem., Int. Ed.* **2019**, *58*, 9491; c) Z. Jiang, X. Xu, Y. Ma, H. S. Cho, D. Ding, C. Wang, J. Wu, P. Oleynikov, M. Jia, J. Cheng, Y. Zhou, O. Terasaki, T. Peng, L. Zan, H. Deng, *Nature* **2020**, *586*, 549; d) J. Zhang, T. Bai, H. Huang, M.-H. Yu, X. Fan, Z. Chang, X.-H. Bu, *Adv. Mater.* **2020**, *32*, 2004747.

[12] a) M. Zhao, K. Yuan, Y. Wang, G. Li, J. Guo, L. Gu, W. Hu, H. Zhao, Z. Tang, *Nature* **2016**, *539*, 76; b) L. Li, Y. Li, L. Jiao, X. Liu, Z. Ma, Y.-J. Zeng, X. Zheng, H.-L. Jiang, *J. Am. Chem. Soc.* **2022**, *144*, 17075.; c) Y. Yun, H. Sheng, K. Bao, L. Xu, Y. Zhang, D. Astruc, M. Zhu, *J. Am. Chem. Soc.* **2020**, *142*, 4126.

[13] a) H. Liu, M. Cheng, Y. Liu, G. Zhang, L. Li, L. Du, B. Li, S. Xiao, G. Wang, X. Yang, *Coord. Chem. Rev.* **2022**, *458*, 214428; b) B. An, Z. Li, Z. Wang, X. Zeng, X. Han, Y. Cheng, A. M. Sheveleva, Z. Zhang, F. Tuna, E. J. L. McInnes, M. D. Frogley, A. J. Ramirez-Cuesta, S. N. Louise, C. Wang, W. Lin, S. Yang, M. Schroder, *Nat. Mater.* **2022**, *21*, 932.

[14] a) Y. Pan, J. Wang, S. Chen, W. Yang, C. Ding, A. Waseem, H.-L. Jiang, *Chem. Sci.* **2022**, *13*, 6696; b) E. Rissi, E. E. Fileti, S. Canuto, *Theor. Chem. Acc.* **2003**, *110*, 360.

[15] a) J. Ran, M. Jaroniec, S.-Z. Qiao, *Adv. Mater.* **2018**, *30*, 1704649; b) X. Hu, Y. Ye, W. Dong, Y. Huang, M. Zhu, *Appl. Catal. B* **2022**, *309*, 121238.

[16] Y. Qian, D. Li, Y. Han, H.-L. Jiang, *J. Am. Chem. Soc.* **2020**, *142*, 20763.

[17] W. Wang, H. Wang, X. Tang, J. Huo, Y. Su, C. Lu, Y. Zhang, H. Xu, C. Gu, *Chem. Sci.* **2022**, *13*, 8679.

[18] H. Wang, X. Sun, D. Li, X. Zhang, S. Chen, W. Shao, Y. Tian, Y. Xie, *J. Am. Chem. Soc.* **2017**, *139*, 2468.

[19] Y. Chen, J. Lin, L. Li, B. Qiao, J. Liu, Y. Su, X. Wang, *ACS Catal.* **2018**, *8*, 859.